AGU PUBLICATIONS

Geochemistry, Geophysics, Geosystems

RESEARCH ARTICLE
10.1002/2015GC006185

Deformation of the Nankai Trough inner accretionary prism: The role of inherited structures

Brian Boston[1], Gregory F. Moore[1], María José Jurado[2], and Hiroki Sone[3,4]

[1]Department of Geology and Geophysics, University of Hawai'i, Honolulu, Hawai, USA, [2]Institute of Earth Sciences Jaume Almera ICTJA, Spanish National Research Council CSIC, Barcelona, Spain, [3]Section 3.2 Geomechanics and Rheology, GFZ German Research Centre for Geosciences, Potsdam, Germany, [4]Now at Geological Engineering Program, Department of Civil and Environmental Engineering, University of Wisconsin-Madison, Madison, Wisconsin, USA

Key Points:
- Inherited structures created at the outer prism are partially preserved within the inner prism
- A reactivated fault within the inner prism indicates a dynamic history
- Steeply dipping beds with multiple fracture populations are found at depth

Correspondence to:
B. Boston,
bboston@hawaii.edu

Citation:
Boston, B., G. F. Moore, M. J. Jurado, and H. Sone (2016), Deformation of the Nankai Trough inner accretionary prism: The role of inherited structures, *Geochem. Geophys. Geosyst.*, *17*, doi:10.1002/2015GC006185.

Received 16 NOV 2015
Accepted 22 JAN 2016
Accepted article online 2 FEB 2016

Abstract Accretionary prisms commonly grow seaward, with the strata of the inner prism consisting of older, previously accreted outer prism rocks overlain by thick fore-arc basin strata. We focus on the Nankai Trough inner accretionary prism using three-dimensional (3-D) seismic data and logging data from the Integrated Ocean Drilling Program (IODP). We update the 3-D seismic volume using well velocity data to better constrain deeper horizons. Interpretation of these horizons reveals multiple folds with axial surfaces that strike near parallel to modern outer prism thrust faults, and we interpret that these folds formed as a result of thrust faulting. Reactivation of one inner prism thrust fault continued until at least ~0.44 Ma, after the modern fore-arc basin formed, indicating that the inner prism had continued deformation until that time. Structural restorations of these folded seismic horizons demonstrate that ~580 m of slip occurred on this steeply dipping reactivated thrust after fore-arc basin formation. Structural interpretation and analysis of logging-while-drilling data, including borehole images, in the deep inner prism revealed intense deformation of a generally homogenous lithology characterized by bedding that dips steeply (60°–90°), intersected by faults and fractures that have a range of dips and densities. Our study of the deep Kumano Basin provides new insights into the structure of the inner prism and reveals that although the inner prism has partially preserved inherited outer prism structures, these older folds and faults are steeply rotated and cut by multiple fracture populations during subsequent deformation.

1. Introduction

In most sediment-dominated subduction zones, kilometers-wide accretionary prisms form by off-scraping marine sediments from the down-going plate. The seaward (outer) portions of accretionary prisms have been extensively studied, and their growth mechanics are well established [e.g., *Davis et al*., 1983; *Dahlen*, 1990]. The older, deeper (inner) portions of accretionary prisms are thought to suffer less internal deformation after potentially being stabilized by the addition of overlying fore-arc basin strata [e.g., *Wang and Hu*, 2006], but there have been few studies to confirm these processes. We focus on the inherited outer prism structures that are later modified in the inner prism environment.

Coulomb wedge theory is typically applied to quantify accretionary prism growth and evolution. The outer accretionary prism grows seaward and thicken through imbricate in-sequence thrust faulting, in which packets of sediments are scraped from the incoming plate at the frontal thrust and added to the overriding plate to form a wedge [*Davis et al*., 1983], and by underplating, which takes place at the base of the prism where sediment from the subducting plate is accreted beneath the base of the prism [*Stockmal*, 1983; *von Huene and Scholl*, 1991; *Platt*, 1986; *Moore and Biju-Duval*, 1984]. In Coulomb wedge theory, the stability of the outer accretionary prism is controlled by the wedge's frictional, material, and fluid dynamic properties along with the dip angle of the décollement [*Davis et al*., 1983; *Dahlen*, 1990; *Suppe*, 2007]. If the wedge is not at the critical taper angle, it will become more stable by internal wedge deformation, most easily achieved by flattening or steepening of the topography [*Davis et al*., 1983; *Lallemand and Lepichon*, 1987; *Kukowski et al*., 2010; *Alves et al*., 2014]. If the prism grows too wide and too rapidly, the surface slope decreases, which in turn decreases the wedge taper, and in order for this wedge to restore its equilibrium taper, out-of-sequence thrusts (OOSTs) may cut the wedge or reactivate older in-sequence thrusts landward of the deformation front to increase the surface slope and wedge taper [*Morley*, 1988]. Coulomb wedge

theory generally assumes a strong static backstop (a region within the fore arc with a greater shear strength than the seaward region [*Byrne et al*., 1993]). However, a dynamic backstop consisting of older accreted sediments can develop further seaward [*Kopp and Kukowski*, 2003], with this new inner accretionary prism remaining stable throughout the earthquake cycle, in contrast to the outer accretionary prism that deforms during the cycle [*Wang and Hu*, 2006].

Many hypotheses have developed for the origin and evolution of a megasplay fault system, or OOST zone. They range from local events, such as seamount or ridge subduction, to regional processes, such as subduction rate or sediment influx, to tectonic inversion of normal faults [*Park et al*., 2004; *Mazzotti et al*., 2002; *Collot et al*., 2008]. In addition to providing a mechanism for wedge thickening and defining the slope of the wedge, OOSTs can lead to the formation of an outer ridge [*Park et al*., 2002; *Moore et al*., 2007; *Gulick et al*., 2010], creating accommodation space at the distal edge of the fore-arc basin for sediment deposition on top of the older accretionary prism [*Underwood and Moore*, 2012]. Shortening from the OOST may be recorded by deformation patterns seen in the fore-arc basin by landward tilted sediments, demonstrating that the creation of OOST faults can influence the formation and growth of the basin [*Gulick et al*., 2010; *Moore et al*., 2015]. Because the inner prism is thought to remain stable throughout the earthquake cycle, this new setting provides a favorable environment for an overlying fore-arc basin to form and develop [*Wang and Hu*, 2006]. These basins tend to correlate with seismically locked regions suggesting a link between upper plate processes and seismic coupling on the plate boundary thrust [*Wells et al*., 2003; *Song and Simons*, 2003; *Fuller et al*., 2006].

The growth and dynamics of the inner accretionary prism are less well understood than those of the juxtaposed outer prism. In contrast to the outer prism that grows seaward through regular accretion of sediments from active in-sequence-faulting, the inner prism grows seaward during less regular events through the formation of OOSTs or megasplay faults [*Park et al*., 2002; *Moore et al*., 2007]. This process leads to a rapid addition of large outer prism sections into the inner prism, moving the inner/outer prism boundary seaward in sudden steps. While the outer prism continues to develop, the inner prism remains stable and does not grow until a new seaward OOST forms [*Strasser et al*., 2009]. The inner prism tectonic setting is clearly distinct from that of the outer prism but with an uncertain role in subduction zone and earthquake processes.

This paper focuses on the inner accretionary prism of the Kumano section of the Nankai Trough. This region has been the focus of multiple seismic cruises and Integrated Ocean Drilling Program (IODP) scientific drill sites. IODP Expedition 338 and 348 drilled deep into the inner accretionary prism off of the Kii Peninsula [*Strasser et al*., 2014; *Tobin et al*., 2015a], providing direct measurements to improve the seismic interpretations at depth. In this paper, we update the 3-D seismic depth volume, make new seismic and logging interpretations, and model fault-related folds. Our goal is to provide new structural constraints on this setting and how inner prism structures inherited during initial accretion are later modified.

2. Tectonic Setting

The Nankai Trough is located south of central Honshu, Japan, where the Philippine Sea Plate (PSP) subducts beneath the Eurasian Plate (Figure 1) at an estimated convergence rate of ~40–60 mm/yr [*Seno et al*., 1993; *DeMets et al*., 2010; *Loveless and Meade*, 2010]. Evidence of long-term accretion extends landward from the trench where Cretaceous and Tertiary accretionary prism units have formed subparallel to the trench axis with imbricated thrust slices analogous to the modern subduction zone [*Taira et al*., 1988]. This margin has one of the longest historical records (~1300 years) of regularly recurring great earthquakes ($M > 8$) at approximately 100–200 year intervals [*Ando*, 1975], including the instrumentally recorded 1944 Tonankai and 1946 Nankaido earthquakes [*Kanamori*, 1972]. These two past events involved coseismic slip on a splay fault [*Baba et al*., 2006; *Baba et al*., 2002], that contributed to the tsunami [*Wendt et al*., 2009].

The Nankai Trough accretionary prism system (Figure 2) is directly influenced by the topography of the incoming plate and its sediment cover. The Shikoku Basin (Figure 1) is the northern margin of the subducting PSP. This basin formed by rifting and back-arc spreading of the Izu-Bonin island arc system during ~25–15 Ma [*Kobayashi and Nakada*, 1978; *Okino et al*., 1994, 1999]. Clockwise rotation of the Shikoku Basin spreading axis occurred during the early to mid-Miocene, followed by late-stage volcanism until the late Miocene that formed large seafloor features, such as the Kinan seamount chain [*Okino et al*., 1994, 1999].

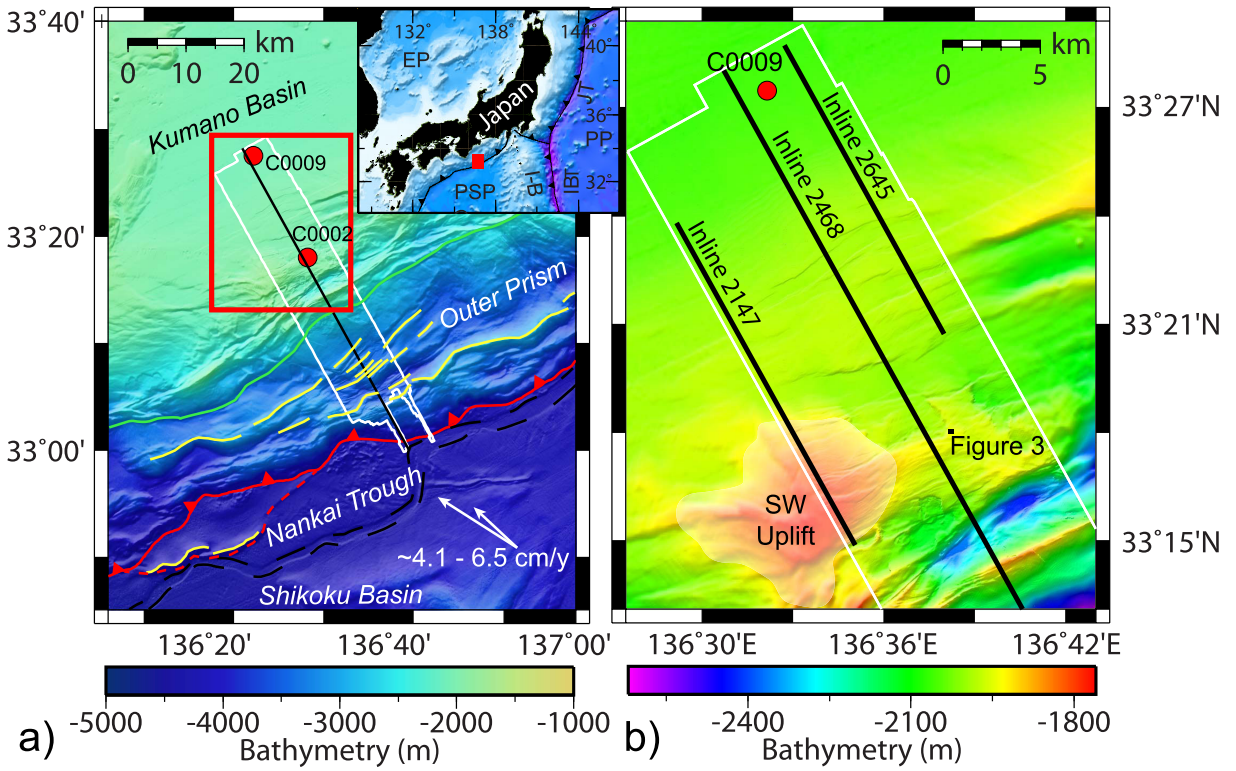

Figure 1. Bathymetric map of the Kumano section of the Nankai Trough. The map shows the locations of IODP drill sites (red dots), the outline of the 3-D seismic volume (white box), and seismic inline (black line). (a) Tectonic interpretation of the Nankai region (modified from *Moore et al.* [2009]). Red solid and dashed lines are the frontal thrust fault and the new frontal thrust fault, respectively. Yellow lines mark the crests of anticlines or ridges. Green line is the out-of-sequence thrust fault. Black dashed lines mark the trench axis channel. Red box is location of Figure 1b. Black line is seismic inline 2468. Inset in the upper right shows the regional tectonic setting of the Nankai Trough with the red box showing the location of the main map—EP = Eurasian Plate; PSP = Philippine Sea Plate; I-B = Izu-Bonin arc; IBT = Izu-Bonin Trench; PP = Pacific Plate; JT = Japan Trench. (b) Study region for this paper. Black lines are seismic inlines shown. Black box is Site C0002 region in Figure 3.

Farther east, the Izu-Bonin-Mariana volcanic arc collided against the Honshu arc ~15 Ma, leading to rapid uplift and erosion with increased sediment flux and deposition down through the Nankai trench axis [*Itoh*, 1988; *Underwood et al.*, 1993]. Terrigenous Miocene turbidites were channeled around variations in the igneous basement relief and into graben and low-lying areas, while leaving basement highs with thin hemipelagic sediments [*Ike et al.*, 2008a,b]. The turbidites filled the trenchward part of the Shikoku Basin, burying the basement relief. The large increase in sediment volume available for accretion led to the outer prism, in parts of the Nankai Trough such as the Muroto and Kumano sections, growing ~40 km perpendicular to the trench [*Moore et al.*, 2001; *Strasser et al.*, 2009]. The influx of sediment changed the structure of the wedge to that of the present day. Based on Coulomb wedge theory, we infer that the prism flattened due to the increased growth from high input at the trench, and in turn resulted in an OOST that thickened and

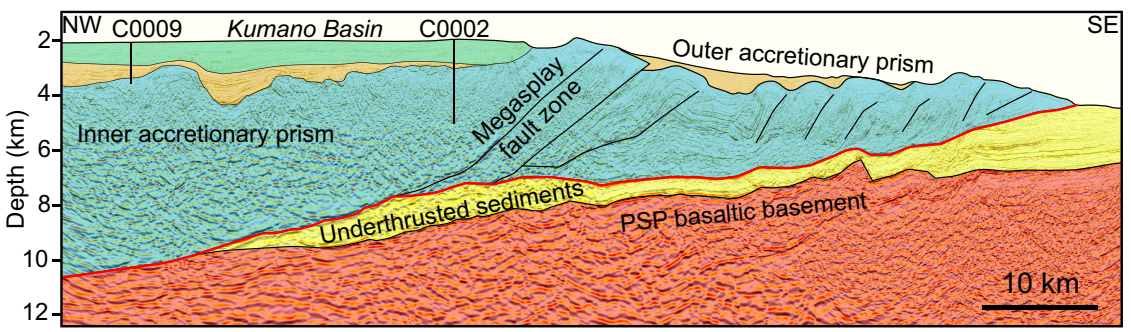

Figure 2. Seismic inline 2468 across the outer and inner accretionary prisms with interpretation based on *Moore et al.* [2014]. PSP = Philippine Sea Plate. Projected drill Sites C0002 and C0009 are also shown. The green and orange units are fore-arc basin fill and slope fill, respectively. The red line is the plate boundary fault.

maintained a critical taper in a self-similar geometry [*Davis et al*., 1983]. This tectonic history likely influenced the OOST system throughout the Nankai Trough.

The Nankai Trough outer prism consists of three main sections from seaward to landward: the frontal thrust zone, the imbricate thrust zone, and the OOST zone [e.g., *Moore et al*., 2009; *Kimura et al*., 2011]. The frontal thrust zone throughout the margin typically consists of a main detachment with dips of ∼30° but with anomalous regions where the frontal thrust has shallow-dips (<10°) [*Gulick et al*., 2004; *Moore et al*., 2009]. Thrust faults within the imbricate thrust zone branch off a basal décollement and remain parallel to the deformation front with similar dips [*Gulick et al*., 2004]. Thrusting within the imbricate thrust zone occurred even at a time with little frontal accretion [*Kinoshita et al*., 2011]. The subducting sediments below the active basal décollement are relatively undeformed from thrust faulting [*McNeill et al*., 2004; *Bangs et al*., 2009; *Tobin and Saffer*, 2009]. The landward boundary of the Nankai Trough outer accretionary prism is the OOST zone. The OOST faulting initiated at ∼1.95 Ma with fluctuating periods of high and low activity [*Strasser et al*., 2009]. The uplift from the OOST fault zone leads to mass-transport deposits and seafloor erosion [*Alves et al*., 2014], and additional erosional processes may be found at imbricate thrusts [*Van Tuyl et al*., 2015], with both altering the critical taper of the prism.

The Kumano Basin is located landward the OOST fault zone on the eastern part of the Nankai Trough (Figure 1) and overlies the thrusts and slope fill of the inner prism (Figure 2). The distal portion of the Kumano Basin is largely defined by landward tilted horizons [*Gulick et al*., 2010; *Moore et al*., 2007] and multiple sets of normal fault populations [*Moore et al*., 2013; *Sacks et al*., 2013]. The evolution of the Kumano fore-arc basin is directly interwoven with OOST formation and uplift, developing from an interplay between tectonics and sedimentation [*Moore et al*., 2015]. The distal edge of the Kumano Basin and underlying accretionary prism comprise five units, based on cores, cuttings, and logs from IODP Sites C0002 and C0009 [*Expedition 314 Scientists*, 2009; *Expedition 319 Scientists*, 2010; *Strasser et al*., 2014]. The upper units (I and II) are considered to be modern Kumano Basin sediments consisting largely of hemipelagic deposits with fine-grained turbiditic sediments [*Expedition 314 Scientists*, 2009; *Expedition 315 Scientists*, 2009]. Unit III contains slope basin deposits that overlie an older accretionary prism (Unit IV) [*Expedition 319 Scientists*, 2010]. Unit IV generally exhibits a chaotic seismic reflection pattern. Unit V is thought to be older Shikoku Basin sediments with the oldest sediments dated at Site C0002 [*Strasser et al*., 2014; *Tobin et al*., 2015a]. Additionally, 12 seismic sequences have also been defined within Unit I/II [*Gulick et al*., 2010] and three seismic sequences within Unit III [*Ramirez et al*., 2015].

3. Data and Methods

3.1. Seismic Data

A three-dimensional (3-D) seismic reflection volume was collected in 2006 aboard the M/V *Nordic Explorer* by Petroleum GeoServices (PGS) off southwest Japan (Figure 1). Acquisition was performed with a two-source array, each consisting of 28 air guns fired alternately at 37.5 m intervals. Four 4500 m long streamer cables were spaced 150 m apart, with 12.5 m spacing of receiver groups for each cable. The resulting seismic volume has an inline spacing of 12.5 m, a crossline spacing of 18.75 m, and a nominal fold of 30. Compagnie Générale de Géophysique (CGG) processed the data through 3-D prestack time migration (PSTM) using traditional data conditioning and multiple reduction, and later, the Japan Agency for Marine Earth Science and Technology (JAMSTEC) performed a 3-D prestack depth migration (PSDM). Due to the relatively short streamer length and strong feathering by the Kuroshio Current, velocity resolution at depth is less accurate than in the shallow section [*Moore et al*., 2009]. Depth processing produced clear images (Figure 2) with a resolution of ∼5–20 m for the Kumano Basin sediments [*Moore et al*., 2009]. This data set extends into the Kumano Basin landward of the OOST (Figure 1) covering a ∼12 km × 25 km area within the basin. Using the 3-D PSDM seismic volume, we mapped individual horizons throughout the basin. Two main boundaries, seismic horizons KL and UC2, were mapped based on onlapping relationships, seismic character, and well data. Additional Kumano Basin horizons were also mapped in 3-D with horizon names following previous labeling schemes [e.g., *Moore et al*., 2015].

3.2. Well Data

IODP drilling with D/V *Chikyu* along the Kumano transect included two well sites within the Kumano Basin (Figure 1). Site C0002 is located near the seaward side of the basin, whereas C0009 is near the landward

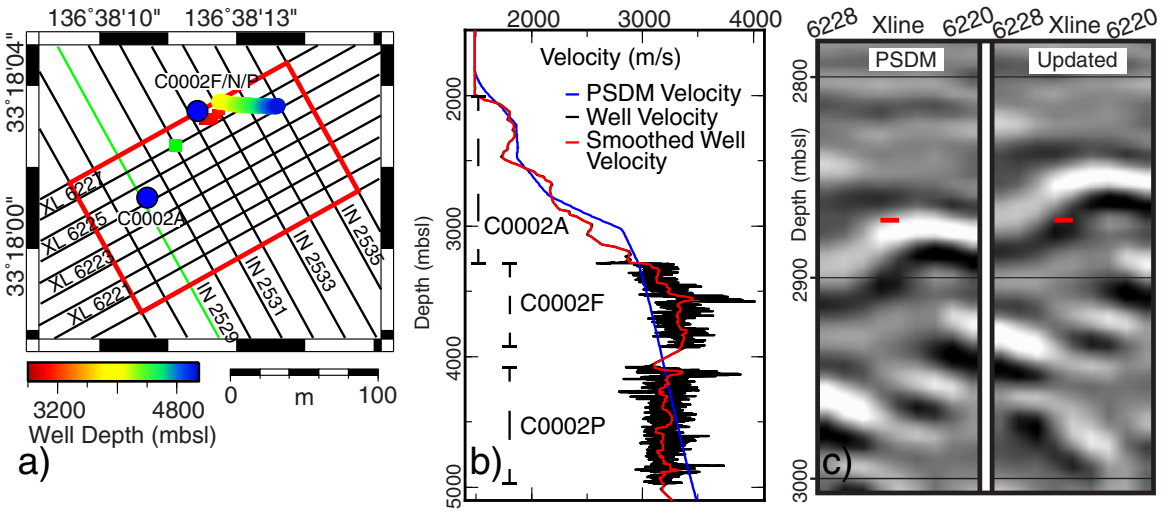

Figure 3. Well compressional velocity and velocity-corrected seismic data. (a) Location of Site C0002 holes (blue circles) and well paths (depth color coded). Red box is region of the seismic update. Green box is the location of PSDM velocity profile shown in Figure 3b. Green line is seismic inline for Figure 3c. (b) Well velocities and PSDM velocity. (c) Original PSDM seismic reflectors (left) compared to the updated seismic reflectors (right) of seismic inline 2529. Red line marks the depth of to the top of Unit IV [*Expedition 314 Scientists*, 2009]. Note that our new velocity model shifts all reflections shallower.

extent of the 3-D survey. Expedition 314 drilled Hole C0002A to 1401 meters below seafloor (mbsf) collecting logging-while-drilling (LWD) data [*Expedition 314 Scientists*, 2009]. Hole C0009A on Expedition 319 collected LWD data and cores [*Expedition 319 Scientists*, 2010]. Expedition 338 extended drilling at Hole C0002F to 2005.5 mbsf and also collected LWD data and borehole images and cores, while Expedition 348 extended Site C0002 to 3058.5 mbsf using sidetracked Hole C0002P collecting a suite of LWD data, including natural gamma ray, electrical resistivity logs and images, sonic velocity, and sonic caliper logs [*Tobin et al*., 2015b].

The focus here is on a subset of Hole C0002P data: the gamma ray log, the resistivity log, resistivity image, and the sonic log. The RH48PC resistivity log is a phase shift resistivity log with a 48 inch sensor spacing collected at 2 MHz frequency [*Tobin et al*., 2015b]. The azimuthal focused resistivity (AFR) produces a high-resolution resistivity image acquired in 128 discrete azimuthal bins with an ideal 10 mm image resolution [*Tobin et al*., 2015b]. The AFR image was filtered with a median 5 × 5 filter to reduce noise. Picks of bedding, faults, and fractures were interpreted from the AFR static image. The sonic log used both a monopole and dipole mode source with a frequency between 2 and 25 kHz and recorded the full waveform signal [*Tobin et al*., 2015b]. We reprocessed the sonic compressional velocity data based on the original raw waveforms.

3.3. Velocity-Corrected Seismic Volume

We created a new 3-D velocity model at Site C0002 using the PSDM water interval velocity, a seismic checkshot survey at C0002A, and LWD sonic data at C0002F/C0002P. The model is based on the smoothed interval velocity data for C0002A [*Expedition 314 Scientists*, 2009]. Velocity data were combined into a one-dimensional (1-D) profile that was then gridded and smoothed into a 3-D velocity cube covering seismic inlines 2527–2536 and crosslines 6220–6228, bounding the location of all the holes at Site C0002 (Figure 3). Seismic scaling of the PSDM seismic data using the well-based velocity cube created the updated depth seismic section. We converted the PSDM volume to time using the original PSDM velocity volume, and then reconverted the time volume back to depth using our updated velocity volume at Site C0002, in order to improve the match between the seismic and borehole data sets.

3.4. Trishear Model

Due to (1) a seafloor multiple reflection that obscures reflections within the older prism section under the fore-arc basin and (2) high angle dips of the strata, seismic interpretations of the deep thrust faults are poorly constrained. We utilize structural restorations to test and verify our interpretations of the seismic reflection data. Our model in this study uses a forward trishear modeling program, LithoTect®, a graphical structural modeling software that uses our interpreted seismic horizons. Trishear is a kinematic model that deforms a triangular zone ahead of the propagating fault tip based on simple shear with a fixed footwall

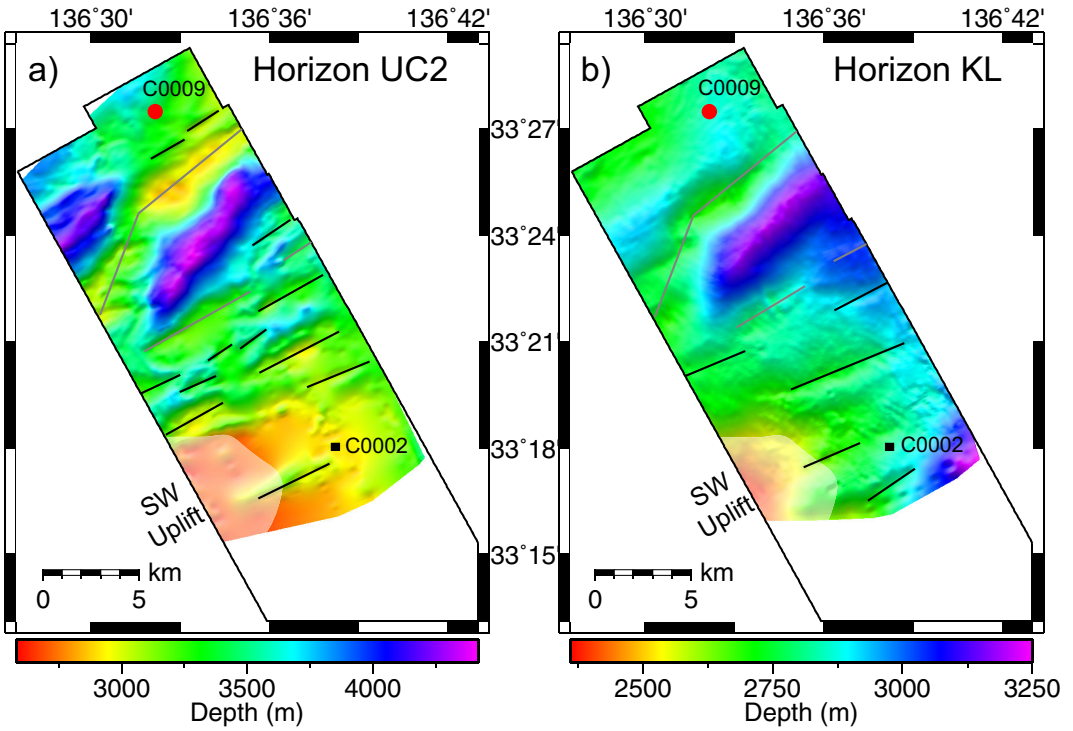

Figure 4. Map view of deep horizons. (a) Horizon UC2 interpreted to be the top of Unit IV. (b) Horizon KL interpreted to be the basal boundary of the modern fore-arc basin. Black box is the limit of the 3-D seismic volume. Black lines mark the main anticlines, and gray lines mark anticlines found at the same positions for both horizons. The SW uplift mapped region is from the bathymetry (Figure 1b).

and a constant-velocity hanging wall [*Erslev*, 1991; *Allmendinger*, 1998]. This model assumes two-dimensional (2-D) deformation within the shear zone based on a velocity field solution by *Zehnder and Allmendinger* [2000]. Kumano Basin fill is generally young, poorly consolidated sediments, which mechanical and kinematic models of folding in comparable environments have created similar deformational patterns [*Hardy and Finch*, 2007]. Fold geometry of the basin fill indicates a trishear-type fault-propagation folding style, allowing for the trishear kinematic approach to estimate fault deformation. Following a forward modeling approach, we estimate trishear parameters, fault geometry, and fault slip by restoring each seismic horizon to a planar footwall slope extended with the same dip as the undeformed seaward part of the same horizon.

4. Results

We focus on a regional to borehole-scale study of the deep inner accretionary prism. We present results of 3-D seismic interpretation, structural interpretation, modeling that tests our interpretation, and deep borehole structural data from the inner prism at the Nankai Trough to illuminate margin processes.

4.1. Top of the Miocene Prism

Because velocities in the updated seismic volume are slightly lower than those of the original PSDM, the new depths for seismic reflections at the base of the fore-arc basin are ~20 m shallower than in the original PSDM volume (Figure 3). The depth at the top of Unit IV at Hole C0002A is 2871.6 meters below sea level (mbsl) from previous LWD results [*Expedition 314 Scientists*, 2009]. The updated seismic volume has the LWD based top of Unit IV clearly correlated to a positive (black) seismic reflection, with the previous PSDM being a negative (white) reflection. The positive reflection agrees with the increase in velocity from Unit III to Unit IV. Using the updated seismic volume and LWD well tie, we can make a confident and precise seismic interpretation of the top of Unit IV, labeled seismic horizon UC2. Because our updated velocity model is limited to the well site, we use the PSDM volume to extrapolate an interpretation of seismic horizon UC2 throughout the full volume (Figure 4). Additionally, we use Site C0009 to help constrain the landward portion of UC2.

UC2 is an unconformity surface that overlies generally discontinuous seismic returns. We use the seismic character to additionally help define UC2, above which continuous reflections from slope basin strata onlap or truncate onto a discontinuous seismic basement. Where a seismic reflection defines the boundary, the reflection is positive, in agreement with the updated seismic volume at Site C0002. This adds confidence to our interpretation of seismic horizon UC2. The final horizon map is smoothed using a 100 m Gaussian filter.

Horizon UC2's morphology is one of the most irregular within the Kumano Basin, with its depth varying by ~1800 m (Figure 4a). The southwestern section of UC2 is the shallowest and corresponds to an area of southwestern local uplift previously documented within the upper seismic sections and seafloor (Figure 1) [*Gulick et al*., 2010; *Moore et al*., 2015]. However, UC2 contains additional folds that are not found on the seafloor within this area, indicating this deformation of UC2 existed before the southwestern uplift event and that different processes created folds and the southwestern uplift. Multiple small-scale folds with wavelengths of ~1–2 km and amplitudes as great as ~500 m are abundant in the southern section. The axial surfaces of these folds strike ~50°–70°, similar to the strike of the outer prism's thrust faults and the local trend of the Nankai Trough. In the northwestern section of the survey, the largest anticline occurs, with more than 1 km of relief; it is marked in Figure 4 by the angular trace of the axial surface. The northeast portion of its crest trends ~50° and the southwest portion trends ~20° Two main synclines flank this anticline, with one south and one northwest of the anticline crest. Horizon UC2 shows clear similarities to the modern outer prism seafloor, indicating that these folds are from imbricate thrusts.

We also map the top of Unit III (slope fill), seismic horizon KL (Figure 4b). This horizon, which marks the top of the slope basin and early Kumano Basin deposits [*Ramirez et al*., 2015], is onlapped by the tilted Kumano Basin fill. Horizon KL is neither horizontal nor planar but exhibits ~900 m of relief. Similar folds are found at the same positions in map view for both horizons KL and UC2. Although horizon KL was tilted during Kumano Basin formation [*Moore et al*., 2015], these folds indicate that the same basement structures that deformed horizon UC2 were active before fore-arc basin deposition, as folds near Site C0002 are not found in the Kumano Basin fill. Horizon KL no longer follows a wedge morphology, indicating uplift and tilting occurred as the OOST formed and changed the tectonic setting of KL from the outer prism to the inner prism.

Analysis of cores and cuttings from Site C0002 revealed increasing depositional ages with depth. The fore-arc basin fill is all Quaternary (<2 Ma) in age [*Expedition 315 Scientists*, 2009; *Strasser et al*., 2014; *Tobin et al*., 2015a]. The underlying trench slope sediments are Pliocene in age and are unconformable with a deformed upper Miocene accretionary prism basement [*Expedition 315 Scientists*, 2009; *Strasser et al*., 2014]. This Miocene prism also reveals increasing ages with depth, and the bottom of Hole C0002P contains depositional ages of ~10 Ma [*Tobin et al*., 2015a; *Strasser et al*., 2014]. Biostratigraphic analyses of nearby Site C0009 also indicate sediments below UC2 are Miocene in age [*Expedition 319 Scientists*, 2010].

4.2. Inner Prism Thrusts

4.2.1. Interpreting Inner Prism Thrusts

We find similar fold-and-thrust structures within the inner prism and the outer prism. However, no thrust fault is directly imaged within the inner prism because the fault dips are too great to be imaged with seismic reflection. Whereas the megasplay fault and décollement associated with the outer prism produce prominent reflections (Figure 2) [*Bangs et al*., 2009; *Moore et al*., 2007], only tilted and folded horizons are preserved within the inner prism on the western portion of the 3-D seismic volume (Figure 5), which is a typical deformational style of the outer prism but with steeper horizons. However, these folds are not continuous throughout the volume, with most of the Miocene prism containing chaotic reflections. These deformed horizons correlate with UC2 folds. We interpret these folded packages to be bounded by thrust faults formed when they were located at the outer accretionary prism and have been incorporated into the inner accretionary prism after the formation of the OOSTs.

4.2.2. Reactivated Thrust Beneath the Kumano Basin

On the landward side of the 3-D seismic volume, the fore-arc basin strata show a more complex structure than just tilting. The KL unconformity surface and underlying slope fill sediments are warped over a basement fault block of accretionary prism sediments (Figure 6). Slope fill strata thin over the top of the fault block, where the strata are deformed into an anticline. Deep slope fill horizons are continuous on the

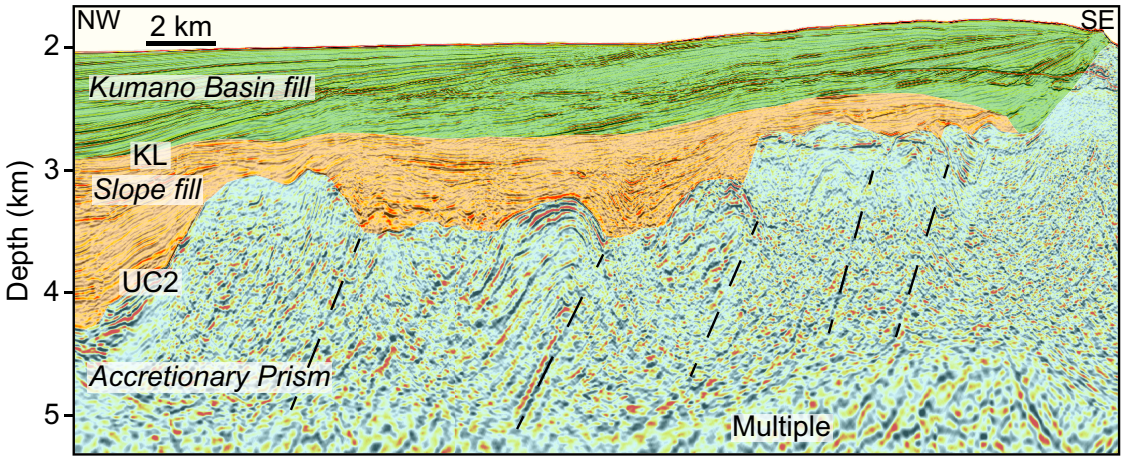

Figure 5. Seismic inline 2147 through the Kumano Basin, location shown in Figure 1b. Buried anticlines are still preserved in some locations, and slope fill shows local deformation. Dashed lines are inferred faults based on folded horizons and slope fill deformation.

southeastern side of the anticline but terminate next to the chaotic horizons of the accretionary prism (Figure 6b). Above these deep horizons, the slope fill consists of growth strata and syndepositional deformation as dips vary with depth, indicating this structure is a thrust fault that was active during sedimentation. Late stage slope basin fill [*Ramirez et al*., 2015] is also tilted. Slope fill seaward of the anticline in Figure 6b is the thickest in the survey at >1000 m thick. From slope fill deformational and depositional patterns, we interpret a deep inner prism thrust fault that initially formed at the outer prism and was active during slope basin formation.

This type of deformation is expected in the outer accretionary prism; however, continued thrusting beneath the modern fore-arc basin is not, as the inner prism is thought to remain stable [*Wang and Hu*, 2006]. Fore-arc basin fill strata are largely characterized by landward tilted horizons, which resulted from uplift by the OOST faults [*Park et al*., 2002; *Gulick et al*., 2010]. However, one region additionally has folded horizons within the Kumano Basin fill (Figure 6). The intensity of folding increases with depth, with shallow horizons only being tilted and the deeper horizons having the greatest folding. This folded region is located above a buried thrust fault (Figure 6b). Due to the deformational style and thrust fault location, we interpret that this fault was reactivated after fore-arc basin formation to cause uplift and folding while the overlying basin filled. Horizon K4 extends to Site C0002 where it correlates with sediments dated to ~0.44 Ma [*Moore et al*., 2015]. This indicates the reactivated fault persisted until <0.44 Ma, as horizons above K4 are also folded.

4.2.3. Kinematic Model of Recent Uplift

We performed multiple iterations of trishear structural restoration [*Zehnder and Allmendinger*, 2000] to test our interpretation of a reactivated thrust fault and to obtain slip and dip information for the fault (Figure 7). The model that performed best used a steeply dipping reverse fault of ~70°, a concentric slip line model for hanging wall deformation, a trishear apical angle of 50°, and a P/S (propagation of fault tip to slip) ratio of 1.25. We added a fault kink to include both the interpretations within the slope basin and reactivated fault tip and geometry. Only three seismic horizons were previously correlated to dated samples from Site C0002: K4 (~0.44 Ma), K5 (~0.9 Ma), and K5b (~1.04 Ma) [*Moore et al*., 2015]. No samples of the upper basin at Site C0009 are available to provide additional age constraints in this region. The fault is currently not active because horizons between K2 and the seafloor are not discernibly folded, and these horizons were not modeled. For horizons dated <0.44 Ma, we estimate a total slip of ~90 m using our trishear model. Horizons dated between ~0.44 and 1.04 Ma have a total slip of ~490 m. For the restoration of the slope fill and UC2, we used a higher P/S ratio of 5 with an apical angle of 60°, for the best modeled results, and found slip of ~660 and ~1000 m, respectively. Finally, we block rotated the restored UC2 20° clockwise around the center point to remove regional tilting caused by the OOST and to estimate the original fault geometry. Our model performed best with a deep fault tip and indicates that during fault reactivation the fault tip did not propagate into the slope sediments. However, our interpreted fault geometry with a kink near the fault tip is similar to the modern fault-bend folds of the outer prism [e.g., *Moore et al*., 1991].

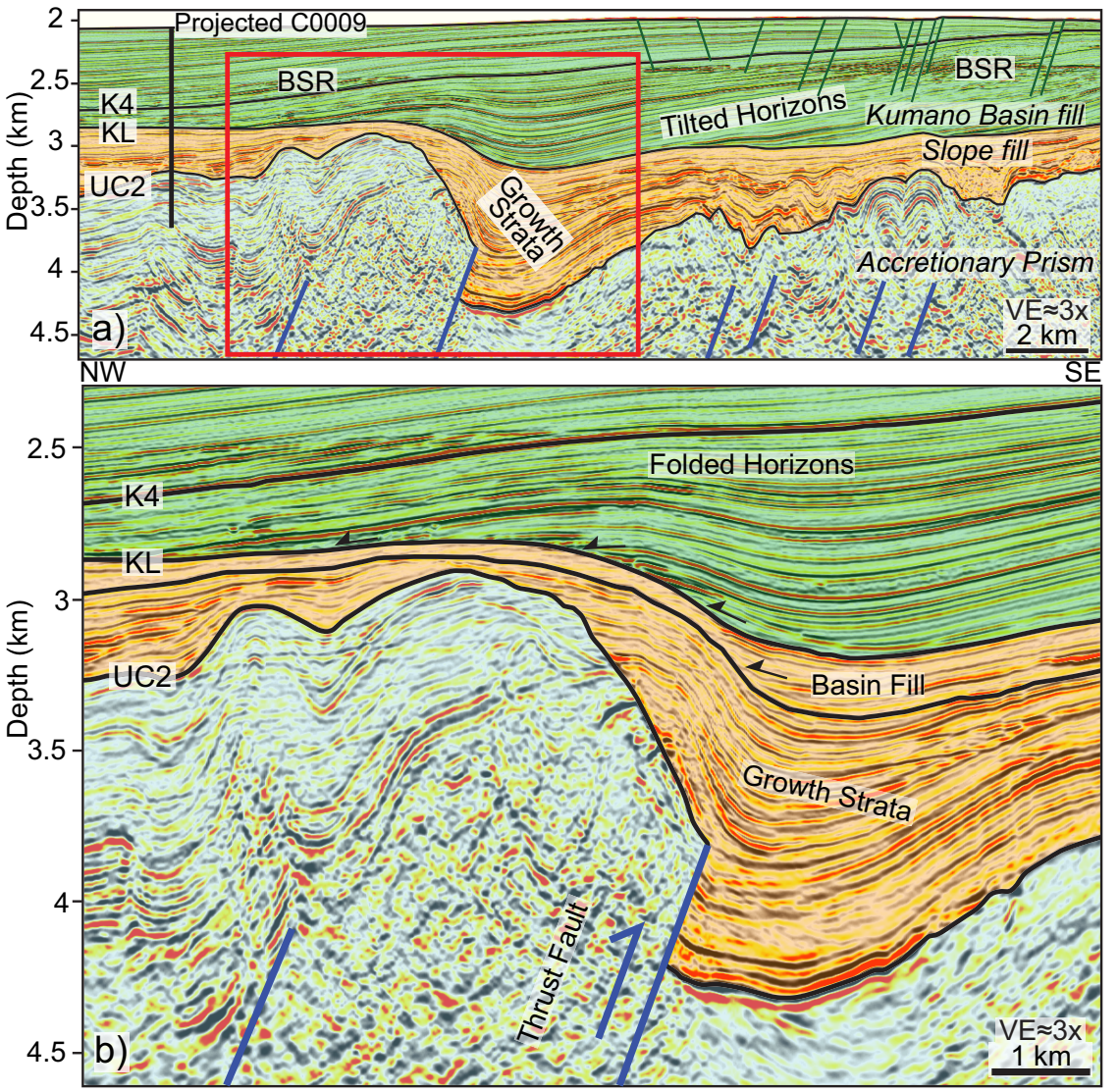

Figure 6. Reactivated buried thrust within the inner prism. Thin black lines are normal faults, and thick blue lines are thrust faults. (a) Seismic inline 2645 across northern anticline and interpretation. Red box is location of Figure 6b. (b) Seismic section shows clear growth strata from thrust uplift within the slope fill. However, Kumano Basin fill is also uplifted within this region. Black arrows indicate onlap.

4.3. Interior of the Inner Prism

The seismic data do not clearly image the deep inner prism, so we analyze borehole-scale LWD data from Hole C0002P to better understand the deep inner prism processes. The small range in data values for the gamma ray, resistivity, and sonic logs indicate a fairly homogenous logged interval (Figures 8a and 8b). We reinterpreted bedding and structural data in Hole C0002P from the resistivity image log (Figure 8c). We find steeply dipping beds with an average dip of $\sim$70° and a range from $\sim$30° to 90°, with bedding strike perpendicular to the convergence direction (Figures 8d and 9a). Faults were picked where offsets were observed, whereas fractures show a break in the bedding with no discernible offsets. Fault and fracture attitudes are more variable than bedding attitudes (Figures 9a and 9b), indicating that multiple phases of deformation occurred in this region. We separately mark additional inferred structures based on variations in interpreted bedding attitude for adjacent beds (Figure 9c). These structures are identified where bedding strike exhibits a change in azimuth of $>$90° or bedding dip changes $\geq$10° with no fracture or fault interpreted between beds. These inferred structures are plotted to show estimated depth locations in the hole. Whereas changes in bedding orientation could

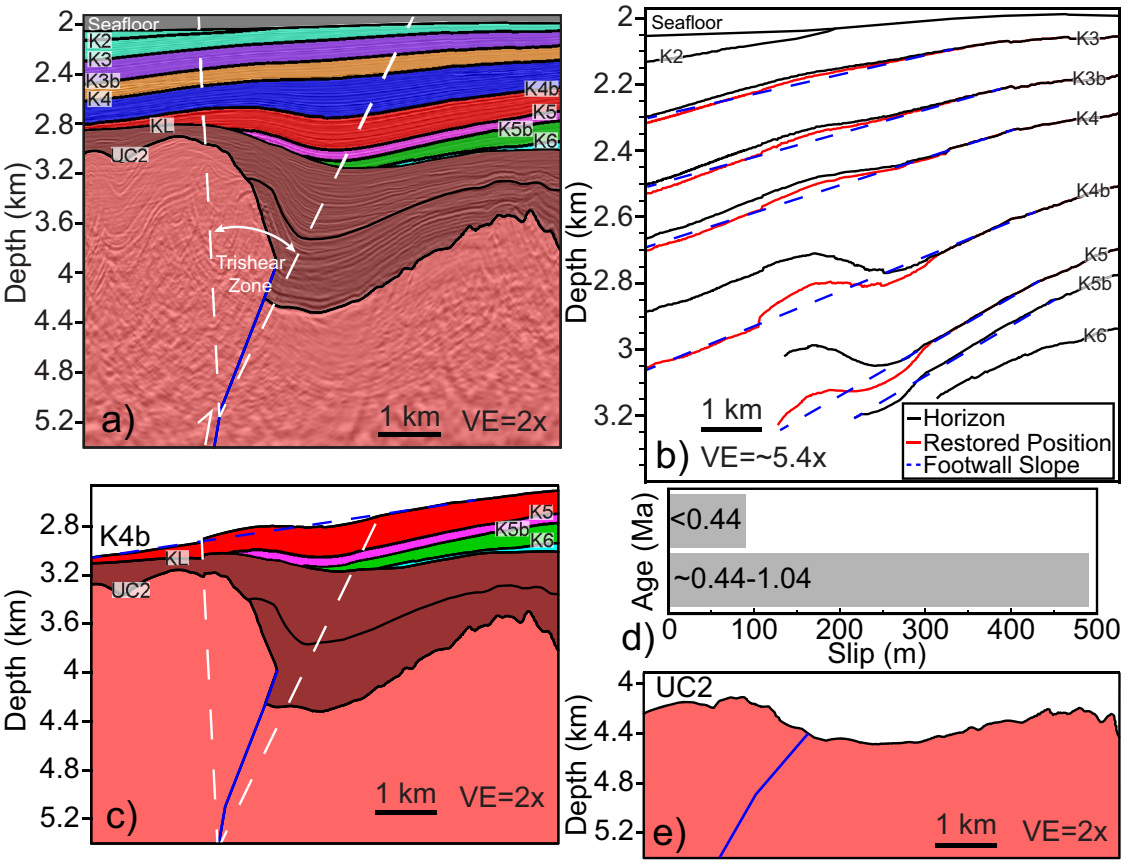

Figure 7. Structural restoration on seismic inline 2645 (Figure 6) using a kinematic trishear model. (a) Interpretation of thrust (blue solid line) and horizons (black lines). Three horizons are dated: K4 (~0.44 Ma), K5 (~0.9 Ma), and K5b (~1.04 Ma). (b) Trishear restoration of each horizon. The amount of restored slip for each horizon was—K3: 20 m; K3b: 30 m; K4: 40 m; K4b: 180 m; K5: 310 m. The seafloor and K2 did not need to be restored. Horizon K5b and K6 did not require additional restoration after restoring overlying horizons, but are also poorly constrained by the fold. (c) Model view of the restoration of horizon K4b. (d) Cumulative fault slip for each binned age range from the restoration. (e) Restoration of UC2, with a 20° block rotation applied.

be related to stratigraphy, based on the local geology, we assume that they reflect structural features, and we interpret them to be from folding or faulting occurring between imaged beds. These additional structural features help to fill gaps in lower quality sections of the image log. The highest density of structures is found at ~2700 mbsf (Figure 9c). This corresponds with both a spike and change in trend in the resistivity log. Two large groups of structural features are found from ~2575–2625 to ~2675–2800 mbsf. These results indicate that the deep interior of the inner prism was subsequently deformed after these strata were inherited from the outer prism.

To better understand the log characteristics of the inner prism, we estimate the true stratigraphic thickness for bedding at C0002P, using the Setchell equation:

$$\mathrm{TST} = \mathrm{MT}(\cos\psi - \sin\psi\ \cos\alpha\ \tan\varphi)\cos\varphi,$$

where TST is true stratigraphic thickness, MT is the measured thickness, ψ is borehole inclination, α is the difference between borehole azimuth and dip azimuth, and φ is the bed dip [*Tearpock and Bischke*, 1991]. Using the interpreted bedding geometry (Figure 8d) and the minimum curvature well path for C0002P (Figure 3a), we applied this equation to each bed interval. Our measured section is 892 m, from the first interpreted bed to the last, with a calculated total true stratigraphic thickness for this same interval of 285 m. This stratigraphic thickness is significantly smaller than the measured interval and may explain the fairly homogenous lithological character from both the logs and the cuttings, as the well path penetrated this stratigraphic section for an additional 607 m due to the steeply dipping beds.

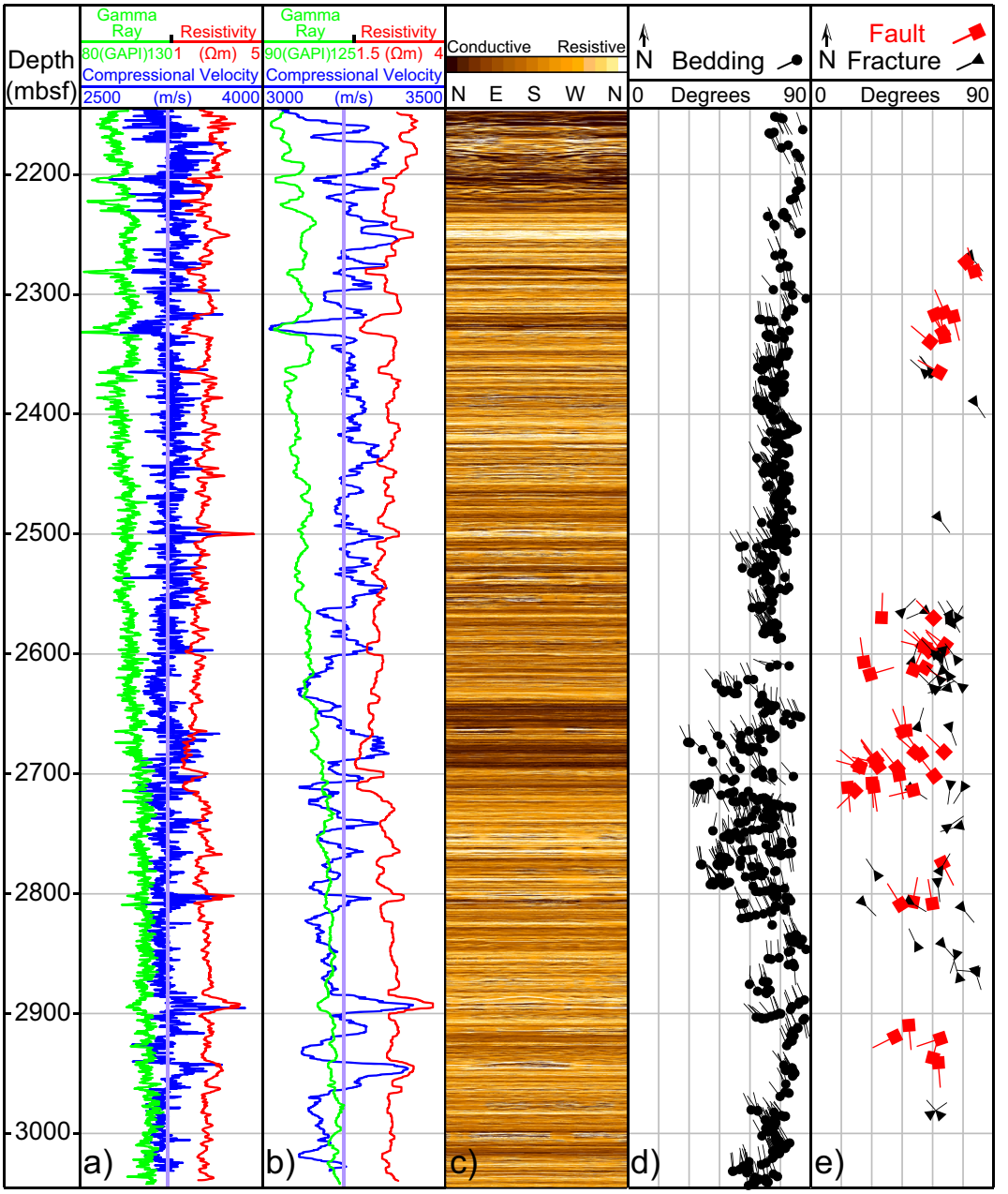

Figure 8. LWD logs from Hole C0002P. (a) Gamma ray in green (left half), resistivity in red (right half), and compressional velocity in blue (full width) with Figure 8b being a smoothed version of the logs using a ~15 m median filter, note the smaller scales. Light blue line in Figures 8a and 8b is a constant velocity of 3220 m/s. (c) Static resistivity image log. Interpretation of (d) bedding and (e) faults and fractures from the resistivity image are plotted as a tadpole diagram.

5. Discussion

The folded and thrusted rocks that comprise the basement of the Kumano Basin form the majority of the inner accretionary prism (Figure 2). Seismic imaging of folds and horizons in the Miocene inner prism is poor but with some features clearly present (Figure 5). The preservation pattern of seismic horizons suggests that deformation within the inner prism is not uniform. Based on our interpretation of the resistivity image from C0002P (Figure 8) and from cores in the upper section [*Tobin et al.*, 2015a], seismic returns within much of the deep inner prism are low due to steeply dipping beds. Additionally, at greater depths, the seismic resolution is lower, and multiple removal techniques performed on the seismic volume

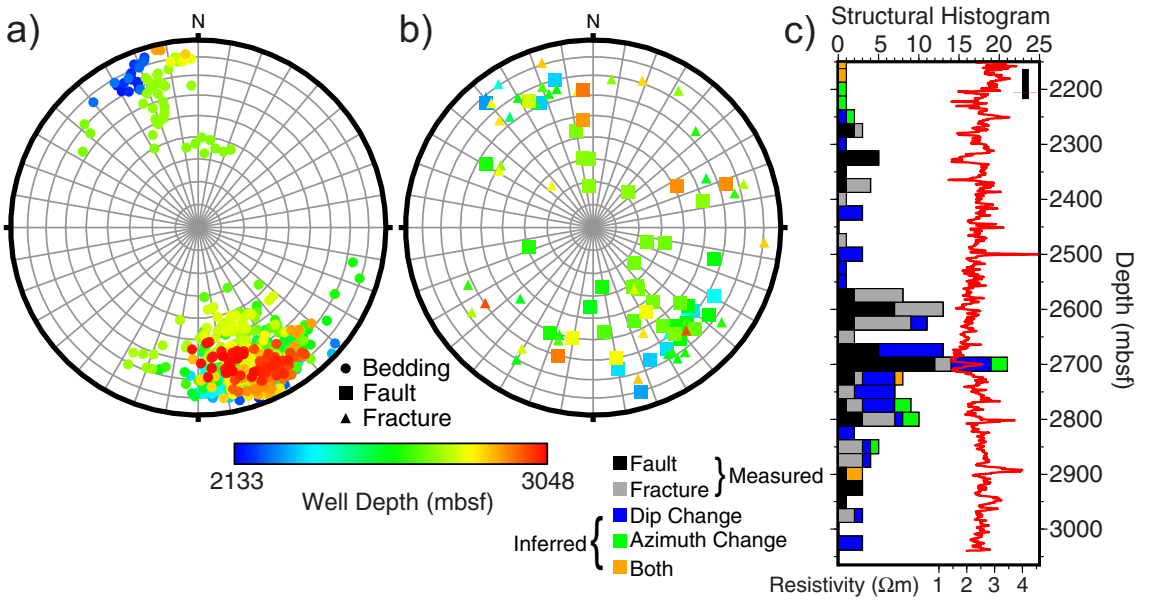

Figure 9. Structure data from Hole C0002P resistivity image log. (a) and (b) are equal area lower hemisphere Schmidt stereonets with poles to bedding planes, fault planes, and fracture planes plotted with depth color coded. (c) Bar plot is a 25 m bin histogram of measured faults and fractures in addition to inferred structures from bedding that are based on bedding dip changes $\geq$10°, bedding azimuth changes >90°, or both. RH48PC resistivity is plotted as red line. Black line is the cored interval.

eliminated high-frequency data below ~5000 mbsl [*Moore et al.*, 2009] leading to poor seismic data quality at depth. However, the presence of some inner prism folds indicates this preservation pattern is not just the result of data processing but is predominately caused from the local geology.

Reactivation of a buried thrust fault (Figure 7) indicates that shortening and compressional stresses continued to persist within the inner prism. Previously collected data from the inner accretionary prism at Sites C0009 and C0002 show a change in the orientation of the maximum principal horizontal stress of nearly 90° between the sites [*Lin et al.*, 2010, 2016]. Numerical models have also shown multiple spatial stress orientations within the inner prism as a consequence of slip on splay faults [*Conin et al.*, 2012]. The presence and location of the reactivated thrust (Figure 6) are consistent with the nearby stress orientation of Site C0009 [*Lin et al.*, 2016, 2010], where the maximum principal horizontal stress orientation at depth is nearly perpendicular to the fault strike. This shows that both the shortening direction from faulting and the stress orientation measured from the well are consistent. The lack of other reactivated thrusts near C0002 in addition to seismic data showing multiple populations of normal faults near C0002 [*Moore et al.*, 2013] is also in agreement with the local maximum horizontal stress at the borehole being nearly parallel to the plate boundary [*Lin et al.*, 2016; *Lin et al.*, 2010]. However, both normal faults within the Kumano Basin fill and the southwestern uplift makes interpretation of thrust fault-related folds within this region difficult. The location of the reactivated thrust fault is consistent with stress orientations found at the well sites; however, the stress state throughout the earthquake cycle is less well defined and may complicate this simple perspective.

The inner prism structure is inherited from initial accretionary deformation. Folds in horizon UC2 and KL (Figure 4) located at the same position indicate that many of these thrust faults that formed them were active until at least the start of fore-arc basin deposition, but became inactive during later stages of fore-arc basin evolution. Although new thrust faults may have cut the prism, the major, mappable features are all inherited or reactivated thrusts (Figures 5 and 6), creating a limit on active inner prism fault geometry. The buried fault tip did not propagate to offset the slope fill during reactivation, in contrast to the modern OOST fault system with fault tips that propagate near the seafloor with little to no slope cover and multiple fault branches [*Strasser et al.*, 2009; *Kimura et al.*, 2011]. The strike of regional structures (Figure 4) and of the deep bedding (Figure 9) within the inner prism are perpendicular to the convergence direction, indicating general preservation of fault strike for the inherited outer prism structures, but the structures have been significantly tilted. Core analysis from Site C0009 suggested that the inner prism rotated ~15° around a vertical axis [*Hayman et al.*, 2012]. The strikes of axial surfaces of many UC2 folds (Figure 4) are within the strike range of the outer prism thrusts, with a fold axis near C0009 having a more northerly strike.

The role of bedding geometry in inner prism stability is unknown. Steeply dipping beds found throughout Hole C0002P (Figure 8) indicate strong deformation before the overlying Kumano Basin fill developed, as the basin sediments are much less deformed, or localized deformation. The bedding strike of the inner prism is generally perpendicular to the plate convergence direction, suggesting that the significant tilting of beds is related to similar collisional processes that formed the outer prism. The steeply dipping prism beds may make for a more stable backstop for outer prism growth. A long-offset walk-away vertical seismic profile at Site C0009 measured a low seismic attenuation factor of *P* waves for the deeper strata, and these results are interpreted to reflect the current stability of the deep inner prism [*Hino et al*., 2015], in agreement with our results.

The seaward edge of the fore-arc basin is still tectonically active with normal faults [*Moore et al*., 2013], strike-slip faults [*Martin et al*., 2010], and the OOST zone [*Strasser et al*., 2009]. Fault and fracture data at Hole C0002P indicate multiple stages of deformation (Figures 8 and 9). The three nearby active fault zones in addition to previous deformation at the outer prism may create the range of fracturing found at Hole C0002P, as these faults and their damage zones may extend to Hole C0002P.

The southwestern uplift of the basin is clearly displayed on the regional bathymetry map (Figure 1) and on maps of horizons KL and UC2 (Figure 4). Our interpretation is that a small basement high subducted underneath this uplifted region, based on the seafloor morphology, as the peak of this region is outside of the 3-D seismic volume. The subducting basement is not imaged properly within this region, and this feature may be within the seismic data's vertical resolution at depth. Similarly, a proposed subducted seamount is inferred to be located east of the 3-D seismic volume [*Kimura et al*., 2011]. However, the southwestern uplift event tilted horizons outside of just the seafloor high region [*Gulick et al*., 2010; *Moore et al*., 2015], and must be related to additional prism processes. We find evidence for inner prism thrusts located within the southwestern uplift region (Figures 4 and 5), but no clear deformation from these faults is found within the overlying Kumano Basin fill. Therefore, inner prism thrust faults do not appear to have been reactivated during this event and consequently did not contribute to the southwestern uplift.

Rapid sedimentation on accretionary prism systems may influence prism development and evolution [e.g., *Simpson*, 2010]. The distal Kumano fore-arc basin formed at an estimated 1.95–2.0 Ma and was initially restricted to a narrow trough seaward of Site C0002 [*Moore et al*., 2015]. At ~1.2 Ma, the basin depocenter started to shift landward as rapid regional uplift and tilting of the basin occurred [*Gulick et al*., 2010; *Moore et al*., 2015]. By the time of deposition of horizon K5b (~1.04 Ma), reactivation of a buried thrust fault started to create localized uplift (Figure 6). This process lead to the basin's depocenter being located near the buried thrust [*Moore et al*., 2015]. As the basin filled and the depocenter shifted landward of the buried thrust (<0.44 Ma), we find that slip decreased on this fault and that the fault recently became inactive (Figure 7). This correlation between fore-arc basin filling and the abandoned reactivated fault suggests that rapid sedimentation of fore-arc basins may play a role in the stability of the inner prism. For instance, rapid sedimentation increases overburden stress, possibly faster than the tectonic loading of the horizontal stress, which would temporarily stabilize the inner prism thrust faults away from criticality.

While the Kumano fore-arc basin formation and evolution is directly affected by the local tectonics [e.g., *Moore et al*., 2015], long-term subsidence will also influence how the basin continues to evolve. The tectonic subsidence curves for fore-arc basins have an assortment of trends, with proposals for these variations ranging from a change in subduction rate or angle, and change in lithospheric thickness and density due to the age and structure of the subducting plate [*Moxon and Graham*, 1987; *Xie and Heller*, 2009]. For the distal Kumano Basin, a reactivated thrust fault (Figure 6) folded strata in the overlying basin, which directly impacted the depocenter and sediment distribution of the basin [*Moore et al*., 2015]. Additionally, large depth variations of UC2 (Figure 4) created an irregular basement for the slope fill and Quaternary Kumano fore-arc basin. In addition to the local tectonics, both the basin's irregular basement depth and the uplift created during basin formation will influence the tectonic subsidence variability of fore-arc basins.

6. Conclusions

In this study, we find that the inner accretionary prism of the Nankai Trough displays both temporal and spatial structural variability. When the boundary between the inner and outer prism steps seaward, thrust faults that originally formed during active accretion at the outer prism become tilted and partially preserved

in the inner prism setting. We mapped and interpreted multiple inner prism thrust faults, and though these faults are currently inactive, we found that one fault was reactivated at ~1.04 Ma, after the OOST formed. Slip along this reactivated fault decreased as the fore-arc basin depocenter shifted over the thrust fault and it became inactive <0.44 Ma. Steeply dipping beds found at depth reflect continued tilting of beds during the formation of the OOST fault, while a range of fracture strikes are interpreted as the result of multiple phases of deformation. Our work reveals that the inner prism does inherit and partially preserve major structures from the outer prism, while also recording the signature of additional deformation.

Acknowledgments

Funding for this research was provided by the National Science Foundation (grant OCE-0451790) and a U.S. Science Support Program Post-Expedition Award. The authors thank the science party of Expedition 348 and are grateful for the support provided by the logging staff scientists (Y. Sanada, Y. Kido, Y. Hamada, and M. K. Thu), the D/V *Chikyu* crew, and technicians. Discussion and comments by C. Conrad and S. Martel greatly improved this manuscript. This research used data provided by the Integrated Ocean Drilling Program (IODP). The Kumano 3-D seismic volume is accessible through the Academic Seismic Portal (http://www-udc.ig.utexas.edu/sdc/). We thank Paradigm Geophysical and Landmark Graphics (Halliburton) for their academic software grants.

References

Allmendinger, R. W. (1998), Inverse and forward numerical modeling of trishear fault-propagation folds, *Tectonics*, *17*(4), 640–656, doi:10.1029/98TC01907.

Alves, T. M., M. Strasser, and G. F. Moore (2014), Erosional features as indicators of thrust fault activity (Nankai Trough, Japan), *Mar. Geol.*, *356*, 5–18, doi:10.1016/j.margeo.2013.07.011.

Ando, M. (1975), Source mechanisms and tectonic significance of historical earthquakes along the Nankai Trough, Japan, *Tectonophysics*, *27*(2), 119–140, doi:10.1016/0040-1951(75)90102-X.

Baba, T., Y. Tanioka, P. R. Cummins, and K. Uhira (2002), The slip distribution of the 1946 Nankai earthquake estimated from tsunami inversion using a new plate model, *Phys. Earth Planet. Inter.*, *132*(1–3), 59–73, doi:10.1016/S0031-9201(02)00044-4.

Baba, T., P. R. Cummins, T. Hori, and Y. Kaneda (2006), High precision slip distribution of the 1944 Tonankai earthquake inferred from tsunami waveforms: Possible slip on a splay fault, *Tectonophysics*, *426*(1-2), 119–134, doi:10.1016/j.tecto.2006.02.015.

Bangs, N. L. B., G. F. Moore, S. P. S. Gulick, E. M. Pangborn, H. J. Tobin, S. Kuramoto, and A. Taira (2009), Broad, weak regions of the Nankai Megathrust and implications for shallow coseismic slip, *Earth Planet. Sci. Lett.*, *284*(1-2), 44–49, doi:10.1016/j.epsl.2009.04.026.

Byrne, D. E., W. Wang, and D. M. Davis (1993), Mechanical role of backstops in the growth of forearcs, *Tectonics*, *12*(1), 123–144.

Collot, J. Y., W. Agudelo, A. Ribodetti, and B. Marcaillou (2008), Origin of a crustal splay fault and its relation to the seismogenic zone and underplating at the erosional north Ecuador–south Colombia oceanic margin, *J. Geophys. Res.*, *113*, B12102, doi:10.1029/2008JB005691.

Conin, M., P. Henry, V. Godard, and S. Bourlange (2012), Splay fault slip in a subduction margin, a new model of evolution, *Earth Planet. Sci. Lett.*, *341-344*, 170–175, doi:10.1016/j.epsl.2012.06.003.

Dahlen, F. A. (1990), Critical taper model of fold-and-thrust belts and accretionary wedges, *Annu. Rev. Earth Planet. Sci.*, *18*, 55–99, doi:10.1146/annurev.earth.18.1.55.

Davis, D., J. Suppe, and F. A. Dahlen (1983), Mechanics of fold-and-thrust belts and accretionary wedges, *J. Geophys. Res.*, *88*(B2), 1153–1172, doi:10.1029/JB088ib02p01153.

DeMets, C., R. G. Gordon, and D. F. Argus (2010), Geologically current plate motions, *Geophys. J. Int.*, *181*(1), 1–80, doi:10.1111/J.1365-246X.2009.04491.x.

Erslev, E. A. (1991), Trishear fault-propagation folding, *Geology*, *19*(6), 617–620, doi:10.1130/0091-7613(1991)019<0617:TFPF>2.3.CO;2.

Expedition 314 Scientists (2009), Expedition 314 Site C0002, in *Proceedings of Integrated Ocean Drilling Program*, vol. 314/315/316, edited by M. Kinoshita et al., Integr. Ocean Drill. Program, Washington, D. C., doi:10.2204/iodp.proc.314315316.114.2009.

Expedition 315 Scientists (2009), Expedition 315 Site C0002, in *Proceedings of Integrated Ocean Drilling Program*, vol. 314/315/316, edited by M. Kinoshita et al., Integr. Ocean Drill. Program, Washington, D. C., doi:10.2204/iodp.proc.314315316.124.2009.

Expedition 319 Scientists (2010), Site C0009, in *Proceedings of Integrated Ocean Drilling Program*, vol. 319, edited by D. Saffer et al., Integr. Ocean Drill. Program, Tokyo, doi:10.2204/iodp.proc.319.103.2010.

Fuller, C. W., S. D. Willett, and M. T. Brandon (2006), Formation of forearc basins and their influence on subduction zone earthquakes, *Geology*, *34*(2), 65–68, doi:10.1130/G21828.1.

Gulick, S. P. S., N. L. B. Bangs, T. H. Shipley, Y. Nakamura, G. Moore, and S. Kuramoto (2004), Three-dimensional architecture of the Nankai accretionary prism's imbricate thrust zone off Cape Muroto, Japan: Prism reconstruction via en echelon thrust propagation, *J. Geophys. Res.*, *109*, B02105, doi:10.1029/2003JB002654.

Gulick, S. P. S., N. L. B. Bangs, G. F. Moore, J. Ashi, K. M. Martin, D. S. Sawyer, H. J. Tobin, S. Kuramoto, and A. Taira (2010), Rapid forearc basin uplift and megasplay fault development from 3D seismic images of Nankai Margin off Kii Peninsula, Japan, *Earth Planet. Sci. Lett.*, *300*(1-2), 55–62, doi:10.1016/j.epsl.2010.09.034.

Hardy, S., and E. Finch (2007), Mechanical stratigraphy and the transition from trishear to kink-band fault-propagation fold forms above blind basement thrust faults: A discrete-element study, *Mar. Pet. Geol.*, *24*(2), 75–90, doi:10.1016/j.marpetgeo.2006.09.001.

Hayman, N. W., T. B. Byrne, L. C. McNeill, K. Kanagawa, T. Kanamatsu, C. M. Browne, A. M. Schleicher, and G. J. Huftile (2012), Structural evolution of an inner accretionary wedge and forearc basin initiation, Nankai margin, Japan, *Earth Planet. Sci. Lett.*, *353-354*, 163–172, doi:10.1016/j.epsl.2012.07.040.

Hino, R., T. Tsuji, N. L. Bangs, Y. Sanada, J.-O. Park, R. von Huene, G. F. Moore, E. Araki, and M. Kinoshita (2015), Q_P structure of the accretionary wedge in the Kumano Basin, Nankai Trough, Japan, revealed by long-offset walk-away VSP, *Earth Planets Space*, *67*(1), 7, doi:10.1186/s40623-014-0175-x.

Ike, T., G. F. Moore, S. Kuramoto, J. O. Park, Y. Kaneda, and A. Taira (2008a), Variations in sediment thickness and type along the northern Philippine Sea Plate at the Nankai Trough, *Isl. Arc*, *17*(3), 342–357, doi:10.1111/j.1440-1738.2008.00624.x.

Ike, T., G. F. Moore, S. Kuramoto, J. O. Park, Y. Kaneda, and A. Taira (2008b), Tectonics and sedimentation around Kashinosaki Knoll: A subducting basement high in the eastern Nankai Trough, *Isl. Arc*, *17*(3), 358–375, doi:10.1111/j.1440-1738.2008.00625.x.

Itoh, Y. (1988), Differential rotation of the eastern part of southwest Japan inferred from paleomagnetism of Cretaceous and Neogene rocks, *J. Geophys. Res.*, *93*(B4), 3401–3411, doi:10.1029/JB093iB04p03401.

Kanamori, H. (1972), Tectonic implications of the 1944 Tonankai and the 1946 Nankaido earthquakes, *Phys. Earth Planet. Inter.*, *5*, 129–139.

Kimura, G., G. F. Moore, M. Strasser, E. Screaton, D. Curewitz, C. Streiff, and H. Tobin (2011), Spatial and temporal evolution of the megasplay fault in the Nankai Trough, *Geochem. Geophys. Geosyst.*, *12*, Q0A008, doi:10.1029/2010GC003335.

Kinoshita, M., G. F. Moore, and Y. N. Kido (2011), Heat flow estimated from BSR and IODP borehole data: Implication of recent uplift and erosion of the imbricate thrust zone in the Nankai Trough off Kumano, *Geochem. Geophys. Geosyst.*, *12*, Q0AD18, doi:10.1029/2011GC003609.

Kobayashi, K., and M. Nakada (1978), Magnetic anomalies and tectonic evolution of the Shikoku inter-arc basin, *J. Phys. Earth*, *26*, 391–402.

Kopp, H., and N. Kukowski (2003), Backstop geometry and accretionary mechanics of the Sunda margin, *Tectonics*, *22*(6), 1072, doi:10.1029/2002TC001420.
Kukowski, N., J. Greinert, and S. Henrys (2010), Morphometric and critical taper analysis of the Rock Garden region, Hikurangi Margin, New Zealand: Implications for slope stability and potential tsunami generation, *Mar. Geol.*, *272*(1-4), 141–153, doi:10.1016/j.margeo.2009.06.004.
Lallemand, S., and X. Lepichon (1987), Coulomb wedge model applied to the subduction of seamounts in the Japan trench, *Geology*, *15*(11), 1065–1069, doi:10.1130/0091-7613(1987)15 < 1065:CWMATT>2.0.CO;2.
Lin, W., et al. (2010), Present-day principal horizontal stress orientations in the Kumano forearc basin of the southwest Japan subduction zone determined from IODP NanTroSEIZE drilling Site C0009, *Geophys. Res. Lett.*, *37*, L13303, doi:10.1029/2010GL043158.
Lin, W., et al. (2016), Distribution of stress state in the Nankai subduction zone, southwest Japan and a comparison with Japan Trench, *Tectonophysics*, doi:10.1016/j.tecto.2015.05.008, in press.
Loveless, J. P., and B. J. Meade (2010), Geodetic imaging of plate motions, slip rates, and partitioning of deformation in Japan, *J. Geophys. Res.*, *115*, B02410, doi:10.1029/2008JB006248.
Martin, K. M., S. P. S. Gulick, N. L. B. Bangs, G. F. Moore, J. Ashi, J. O. Park, S. Kuramoto, and A. Taira (2010), Possible strain partitioning structure between the Kumano fore-arc basin and the slope of the Nankai Trough accretionary prism, *Geochem. Geophys. Geosyst.*, *11*, Q0AD02, doi:10.1029/2009GC002668.
Mazzotti, S., S. J. Lallemant, P. Henry, X. Le Pichon, H. Tokuyama, and N. Takahashi (2002), Intraplate shortening and underthrusting of a large basement ridge in the eastern Nankai subduction zone, *Mar. Geol.*, *187*(1–2), 63–88, doi:10.1016/S0025-3227(02)00245-1.
McNeill, L. C., M. Ienaga, H. Tobin, S. Saito, D. Goldberg, J. C. Moore, and H. Mikada (2004), Deformation and in situ stress in the Nankai Accretionary Prism from resistivity-at-bit images, ODP Leg 196, *Geophys. Res. Lett.*, *31*, L02602, doi:10.1029/2003GL018799.
Moore, G. F., D. E. Karig, T. H. Shipley, A. Taira, P. L. Stoffa, and W. T. Wood (1991), Structural Framework of the ODP Leg 131 Area, Nankai Trough, in *Proceedings of Ocean Drilling Program, Initial Reports*, vol. 131, edited by A. Taira et al., 15–20, Ocean Drill. Program, College Station, Tex., doi:10.2973/odp.proc.ir.131.102.1991.
Moore, G. F., et al. (2001), New insights into deformation and fluid flow processes in the Nankai Trough accretionary prism: Results of Ocean Drilling Program Leg 190, *Geochem. Geophys. Geosyst.*, *2*(10), 1058, doi:10.1029/2001GC000166.
Moore, G. F., N. L. Bangs, A. Taira, S. Kuramoto, E. Pangborn, and H. J. Tobin (2007), Three-dimensional splay fault geometry and implications for tsunami generation, *Science*, *318*(5853), 1128–1131, doi:10.1126/science.1147195.
Moore, G. F., et al. (2009), Structural and seismic stratigraphic framework of the NanTroSEIZE Stage 1 transect, in *Proceedings of Integrated Ocean Drilling Program*, vol. 314/315/316, edited by M. Kinoshita et al., Integr. Ocean Drill. Program, Washington, D. C., doi:10.2204/iodp.proc.314315316.102.2009.
Moore, G. F., B. B. Boston, A. F. Sacks, and D. M. Saffer (2013), Analysis of normal fault populations in the Kumano Forearc Basin, Nankai Trough, Japan: 1. Multiple orientations and generations of faults from 3-D coherency mapping, *Geochem. Geophys. Geosyst.*, *14*, 1989–2002, doi:10.1002/ggge.20119.
Moore, G. F., K. Kanagawa, M. Strasser, B. Dugan, L. Maeda, and S. Toczko (2014), IODP Expedition 338: NanTroSEIZE Stage 3: NanTroSEIZE plate boundary deep riser 2, *Sci. Drill.*, *17*, 1–12, doi:10.5194/sd-17-1-2014.
Moore, G. F., B. B. Boston, M. Strasser, M. B. Underwood, and R. A. Ratliff (2015), Evolution of tectono-sedimentary systems in the Kumano Basin, Nankai Trough forearc, *Mar. Pet. Geol.*, *67*, 604–616, doi:10.1016/j.marpetgeo.2015.05.032.
Moore, J. C., and B. Biju-Duval (Eds.) (1984), Tectonic synthesis, Deep Sea Drilling Project Leg 78A: Structural evolution of offscraped and underthrust sediment, northern Barbados Ridge complex, in *Initial Reports of Deep Sea Drilling Project*, vol. 78A, 601–621, U.S. Gov. Print. Off., Washington, D. C., doi:10.2973/dsdp.proc.78a.133.1984.
Morley, C. K. (1988), Out-of-Sequence Thrusts, *Tectonics*, *7*(3), 539–561, doi:10.1029/TC007i003p00539.
Moxon, I. W., and S. A. Graham (1987), History and controls of subsidence in the Late Cretaceous-Tertiary Great Valley forearc basin, California, *Geology*, *15*(7), 626–629, doi:10.1130/0091-7613(1987)15 < 626:HACOSI>2.0.CO;2.
Okino, K., Y. Shimakawa, and S. Nagakoa (1994), Evolution of the Shikoku Basin, *J. Geomagn. Geoelectr*, *46*, 463–479.
Okino, K., Y. Ohara, S. Kasuga, and Y. Kato (1999), The Philippine Sea: New survey results reveal the structure and the history of the marginal basins, *Geophys. Res. Lett.*, *26*(15), 2287–2290, doi:10.1029/1999GL900537.
Park, J.-O., T. Tsuru, S. Kodaira, P. R. Cummins, and Y. Kaneda (2002), Splay fault branching along the Nankai subduction zone, *Science*, *297*(5584), 1157–1160, doi:10.1126/science.1074111.
Park, J.-O., G. F. Moore, T. Tsuru, S. Kodaira, and Y. Kaneda (2004), A subducted oceanic ridge influencing the Nankai megathrust earthquake rupture, *Earth Planet. Sci. Lett.*, *217*(1-2), 77–84, doi:10.1016/S0012-821X(03)00553-3.
Platt, J. P. (1986), Dynamics of orogenic wedges and the uplift of high-pressure metamorphic rocks, *Geol. Soc. Am. Bull.*, *97*(9), 1037–1053, doi:10.1130/0016-7606(1986)97 < 1037:DOOWAT>2.0.CO;2.
Ramirez, S. G., S. P. S. Gulick, and N. W. Hayman (2015), Early sedimentation and deformation in the Kumano forearc basin linked with Nankai accretionary prism evolution, southwest Japan, *Geochem. Geophys. Geosyst.*, *16*, 1616–1633, doi:10.1002/2014GC005643.
Sacks, A., D. M. Saffer, and D. Fisher (2013), Analysis of normal fault populations in the Kumano forearc basin, Nankai Trough, Japan: 2. Principal axes of stress and strain from inversion of fault orientations, *Geochem. Geophys. Geosyst.*, *14*, 1973–1988, doi:10.1002/ggge.20118.
Seno, T., S. Stein, and A. E. Gripp (1993), A model for the motion of the Philippine Sea plate consistent with Nuvel-1 and geological data, *J. Geophys. Res.*, *98*(B10), 17,941-17,948, doi:10.1029/93JB00782.
Simpson, G. D. H. (2010), Formation of accretionary prisms influenced by sediment subduction and supplied by sediments from adjacent continents, *Geology*, *38*(2), 131–134, doi:10.1130/G30461.1.
Song, T. R., and M. Simons (2003), Large trench-parallel gravity variations predict seismogenic behavior in subduction zones, *Science*, *301*(5633), 630–633, doi:10.1126/science.1085557.
Stockmal, G. S. (1983), Modeling of large-scale accretionary wedge deformation, *J. Geophys. Res.*, *88*(B10), 8271–8287, doi:10.1029/JB088ib10p08271.
Strasser, M., et al. (2009), Origin and evolution of a splay fault in the Nankai accretionary wedge, *Nat. Geosci.*, *2*(9), 648–652, doi:10.1038/ngeo609.
Strasser, M., et al. (Eds.) (2014), Site C0002, in *Proceedings of Integrated Ocean Drilling Program*, vol. 338, Integr. Ocean Drill. Program, Yokohama, Japan, doi:10.2204/iodp.proc.338.103.2014.
Suppe, J. (2007), Absolute fault and crustal strength from wedge tapers, *Geology*, *35*(12), 1127–1130, doi:10.1130/G24053A.1.
Taira, A., J. Katto, M. Tashiro, M. Okamura, and K. Kodama (1988), The Shimanto Belt in Shikoku Japan: Evolution of a Cretaceous to Miocene accretionary prism, *Mod. Geol.*, *12*, 5–46.
Tearpock, D. J., and R. E. Bischke (1991), *Applied Subsurface Geological Mapping*, Prentice Hall, Upper Saddle River, Englewood Cliffs, N. J.

Tobin, H., et al. (Eds.) (2015a), Site C0002, in *Proceedings of Integrated Ocean Drilling Program*, vol. 348, Integr. Ocean Drill. Program, College Station, Tex., doi:10.2204/iodp.proc.348.103.2015.

Tobin, H., et al. (Eds.) (2015b), Methods, in *Proceedings of Integrated Ocean Drilling Program*, vol. 348, Integr. Ocean Drill. Program, College Station, Tex., doi:10.2204/iodp.proc.348.102.2015.

Tobin, H. J., and D. M. Saffer (2009), Elevated fluid pressure and extreme mechanical weakness of a plate boundary thrust, Nankai Trough subduction zone, *Geology*, *37*(8), 679–682, doi:10.1130/G25752A.1.

Underwood, M. B., and G. F. Moore (2012), Evolution of sedimentary environments in the subduction zone of southwest Japan: Recent results from the NanTroSEIZE Kumano transect, in *Tectonics of Sedimentary Basins: Recent Advances*, edited by C. Busby and A. Azor, 310–326, Wiley-Blackwell, N. Y., doi:10.1002/9781444347166.ch15.

Underwood, M. B., R. Orr, K. Pickering, and A. Taira (1993), Provenance and dispersal patterns of sediments in the turbidite wedge of Nankai Trough, in *Proceedings of Ocean Drilling, Scientific Results*, vol. 131, edited by I. A. Hill et al., 15–34, Ocean Drill. Program, College Station, Tex., doi:10.2973/odp.proc.sr.131.105.1993.

Van Tuyl, J., T. M. Alves, and G. F. Moore (2015), Strain decoupling reveals variable seismogenic risk in SE Japan (Nankai Trough), *Geochem. Geophys. Geosyst.*, *16*, 2025–2037, doi:10.1002/2015GC005778.

von Huene, R., and D. W. Scholl (1991), Observations at convergent margins concerning sediment subduction, subduction erosion, and the growth of continental crust, *Rev. Geophys.*, *29*(3), 279–316.

Wang, K. L., and Y. Hu (2006), Accretionary prisms in subduction earthquake cycles: The theory of dynamic Coulomb wedge, *J. Geophys. Res.*, *111*, B06410, doi:10.1029/2005JB004094.

Wells, R. E., R. J. Blakely, Y. Sugiyama, D. W. Scholl, and P. A. Dinterman (2003), Basin-centered asperities in great subduction zone earthquakes: A link between slip, subsidence, and subduction erosion?, *J. Geophys. Res.*, *108*(B10), 2507, doi:10.1029/2002JB002072.

Wendt, J., D. D. Oglesby, and E. L. Geist (2009), Tsunamis and splay fault dynamics, *Geophys. Res. Lett.*, *36*, L15303, doi:10.1029/2009GL038295.

Xie, X., and P. Heller (2009), Plate tectonics and basin subsidence history, *Geol. Soc. Am. Bull.*, *121*(1/2), 55–64, doi:10.1130/B26398.1.

Zehnder, A. T., and R. W. Allmendinger (2000), Velocity field for the trishear model, *J. Struct. Geol.*, *22*(8), 1009–1014, doi:10.1016/S0191-8141(00)00037-7.